*ANZIAM J.* 57(2015), 89–113
doi:10.1017/S1446181115000176

# TRANSITION TO TURBULENCE FROM PLANE COUETTE FLOW

L. K. FORBES[1]

(Received 8 September, 2014; accepted 3 May, 2015; first published online 22 September 2015)

**Abstract**

Modelling fluid turbulence is perhaps one of the hardest problems in Applied Mathematics. In a recent paper, the author argued that the classical Navier–Stokes equation is not sufficient to describe the transition to turbulence, but that a Reiner–Rivlin type equation is needed instead. This is explored here for the simplest of all viscous fluid flows, the Couette flow, which is a simple shear between two moving plates. It is found that at high wavenumbers, the transition to unstable flow at the critical Reynolds number is characterized by a large number of eigenvalues of the Orr–Sommerfeld equation moving into the unstable zone essentially simultaneously. This would generate high-dimensional chaos almost immediately, and is a suggested mechanism for the transition to turbulence. Stability zones are illustrated for the flow, and a simple asymptotic solution confirms some of the features of these numerical results.

2010 *Mathematics subject classification*: primary 76F20; secondary 65F15.

*Keywords and phrases*: Couette flow, instability, nonNewtonian effects, turbulence.

## 1. Introduction

At low speeds, most fluids flow in a smooth laminar manner, but it is a familiar fact that at higher speeds the motion of the fluid becomes turbulent and disordered. Nevertheless, although everyone has an intuitive grasp of what constitutes a turbulent flow, the physics underlying this phenomenon is not entirely certain and, consequently, mathematical models of turbulence are not yet resolved. Understanding turbulent flows is made more difficult by the fact that they are inherently unsteady and fully three-dimensional, and are characterized by eddies over a wide range of length scales.

There is an enormous amount of literature devoted to the study of turbulence and attempts to include it in models of physical phenomena where it occurs. A survey of much of this work is given by Jiménez [14], and a more detailed account is available in the text by Davidson [5]. The review article by Sreenivasan [33] discusses early

[1]School of Mathematics and Physics, University of Tasmania, Hobart, Tasmania 7004, Australia; e-mail: Larry.Forbes@utas.edu.au.

insights and current uncertainties in the experimental and theoretical understanding of turbulence.

In the late nineteenth century, Osborne Reynolds [25] carried out a series of experiments that showed that water flowing in a glass tube becomes unstable at a value of the Reynolds number $R_e = \rho HV/\mu$ of about 2000, where $\rho$ and $\mu$ were the density and viscosity of the fluid and $H$ and $V$ were characteristic lengths and speeds, respectively. This single dimensionless number $R_e$ has since dominated discussion of laminar and turbulent flow, and a history of its development is given by Rott [28]. Later, Reynolds [26] introduced the technique of separating the fluid velocity vector $\mathbf{q}$ in the Navier–Stokes momentum equation into the sum of its time-averaged value $\bar{\mathbf{q}}$ plus a rapidly-varying component $\mathbf{q}'$ with expectation value zero, so that $\mathbf{q} = \bar{\mathbf{q}} + \mathbf{q}'$, and then averaging the equation over time. The aim is to obtain an equation for the slowly varying component $\bar{\mathbf{q}}$ but, due to the convective nonlinear terms in the Navier–Stokes equation, terms of the form $\sigma_{ij} = -\rho\overline{q_i' q_j'}$ also appear. This is the famous *closure problem* of turbulence: since there is no obvious formula for the so-called *Reynolds stress* term $\sigma_{ij}$, at some level, modelling is required in order to close the system of equations. Early attempts simply treated $\sigma_{ij}$ as an additional viscous stress term involving the slowly varying variables $\bar{\mathbf{q}}$ with an enhanced *eddy viscosity* coefficient, but this was later replaced with more complicated K-*epsilon* type models that make this coefficient a function of flow variables (see Kitsios et al. [15] and Speziale [31]). More recently, elaborate moment-closure models have been developed to represent the Reynolds stress term $\sigma_{ij}$, and make use of techniques from field theory and statistics. Further details on such methods are given in the review articles by Cambon and Scott [3] and McComb [19].

Mathematical models of fluid turbulence in incompressible fluids, including those based on advanced statistical techniques [19], take as their starting point the classical Navier–Stokes equation of conservation of momentum for a viscous fluid. This is generally stated without further explanation. A key assumption in the derivation of Navier–Stokes theory is that there is a linear relationship between the stress tensor $\mathbf{T}$ in the fluid and the strain-rate tensor $\mathbf{D}$, as might be anticipated for small to moderate values $\|\mathbf{D}\|$ of the maximum strain rate. Nevertheless, when the Navier–Stokes equation is used to analyze the stability of simple flows to small perturbations, based on linearized theory, it generally gives predictions in poor agreement with experiment. A detailed discussion of much of this work is available from the text by Drazin and Reid [6]. In this classical approach, some exact solution of the Navier–Stokes equation is first obtained for the velocity vector $\mathbf{q}_0$ and pressure $p_0$. Small perturbations $\mathbf{q}_1$ and $p_1$ are then added to these quantities, and the new velocities and pressures are substituted into the Navier–Stokes equation. Linearization is now undertaken, in which only first-order terms in $\mathbf{q}_1$ and $p_1$ are retained, and this yields a coupled system of linear partial differential equations in these perturbation quantities. These linear equations admit solutions with an exponential dependence on time $t$, of the form $\exp(-i\omega t)$. As a result, a new system of linear equations is obtained, in which the complex number $\omega = \omega_R + i\omega_I$ is an eigenvalue. Clearly, if the imaginary part is negative, $\mathrm{Im}\{\omega\} = \omega_I < 0$, the exponential term in the solutions decays with

https://doi.org/10.1017/S1446181115000176 Published online by Cambridge University Press

time, so that the solution is stable. However, if $\omega_I > 0$, then that particular eigenmode grows exponentially with time and the solution is therefore unstable. As discussed by Bayly and Orszag [2], results on the stability of a particular flow are usually presented in terms of the value of Reynolds number $R_e$ at which the linearized solution first becomes unstable, so that $\omega_I = 0$. For simple viscous flows, this linearized analysis based on eigenvalues $\omega$ typically predicts that the boundary between stable and unstable behaviour occurs at very large values of Reynolds number $R_e$, whereas experiments such as those of Reynolds [25] show that the flow becomes unstable at far smaller values of about $R_e = 2000$.

As a result of this discrepancy, there has been considerable dissatisfaction with linearized stability analyses of this type. Trefethen et al. [35] have argued instead for a theory of "stability without eigenvalues". In this approach, modes which have eigenvalues with negative real parts and therefore decay at large time, might nevertheless grow moderately large at early times: large enough to trigger nonlinear instability. In this way, behaviour that is stable in a classical linearized sense might still be capable of triggering instability leading to turbulence. Objections to the results of linearized eigenvalue analysis have also focused on the fact that, since fluid flow is governed by nonlinear equations, large-amplitude nonlinear structures might develop in the flow, for which no linearized counterpart exists. Such large-scale phenomena have been predicted by Waleffe [37] to occur near walls in turbulent flows, based on solutions to the Navier–Stokes equations. Hof et al. [13] subsequently observed similar events in a turbulent pipe flow. This concept has been developed further by Cherubini et al. [4], who sought the types of initial disturbances that would then give rise to the large-scale coherent structures required. An overview of these structures from a dynamical systems viewpoint is given by Eckhardt [7], and Rabin et al. [22] have used a variational formulation with the Navier–Stokes equations to find optimal conditions for generating these coherent structures. Recently, extreme-value analysis in a statistical framework has been used by Faranda et al. [8] to determine the likelihood of transition to turbulence from various initial conditions.

In a recent paper, Forbes [9] has argued that the Navier–Stokes equations, while often accepted uncritically as governing the behaviour of turbulent flows, may in fact not be appropriate for that purpose. After all, Navier–Stokes theory is predicated on the assumption that there is a *linear* relationship between the stress in the fluid and the rate of strain. This is entirely analogous to Hooke's Law in solid mechanics, and assumes that the local rates of strain in the fluid are small. However, a defining property of turbulence is precisely that strain rates may be large, associated in part with the intense swirling motion and the generation of large vorticity. Forbes [9] included additional *nonlinear* terms in the constitutive relation between stress and strain rate: these are sometimes referred to as "elastic" terms in the rheological literature [30], but regarding them as accounting for material nonlinearity may be more appropriate in the present context. This led to a version of the Reiner–Rivlin equations of viscous flow, which was first developed by Reiner [24] and Rivlin [27] and presented also by Aris [1].

Forbes [9] showed that the Reiner–Rivlin equation has the remarkable property that it predicts exactly the same flow patterns as the Navier–Stokes equation *for planar*

https://doi.org/10.1017/S1446181115000176 Published online by Cambridge University Press

*flow*. However, in the fully three-dimensional case, the material nonlinearity terms in the Reiner–Rivlin equation are the cause of complex additional vorticity, for which Navier–Stokes theory has no equivalent. (This then invalidates "Squire's theorem" [32] for such flows.) Forbes [9] used this equation to study the stability of plane Poiseuille flow to small disturbances which are nevertheless fully three-dimensional. Classical linearization was employed, with the consequent calculation of eigenvalues $\omega$ of the approximate system. It was found that the material nonlinearity terms served as an additional source of instability for the flow, beyond that possible purely in Navier–Stokes theory. Some surprising outcomes were also observed. Whereas Navier–Stokes theory predicts that higher wavenumber disturbances are damped more rapidly, in the Reiner–Rivlin equation, they are precisely the modes that are the most unstable. Furthermore, at high wavenumbers, when the critical Reynolds number is reached at which the flow becomes unstable, this is characterized by a large number of eigenmodes crossing into the unstable zone $\mathrm{Im}\{\omega\} = \omega_I > 0$ almost simultaneously. The real parts of these modes $\mathrm{Re}\{\omega\} = \omega_R$ are not integer multiples of one another, and so the transition to instability would involve high-dimensional quasi-periodic behaviour in the linearized system. It is then highly probable that nonlinear effects would cause this to collapse into a type of high-dimensional chaos, through the Ruelle–Takens–Newhouse bifurcation (see Thompson and Stewart [34, p. 196]); Forbes [9] proposed this as an explanation for the transition from laminar to turbulent flow.

There is a sizeable amount of literature on *elastic instabilities* in more complex rheological flows. These generally involve a much more complicated constitutive law between the stress tensor and the rate of strain tensor, than in the Reiner–Rivlin model [1]. In particular, a time derivative of the stress tensor is usually present (see Shaqfeh [30]), and this term appears to have a stabilizing effect on the linearized system. This is consistent with the findings of Lee and Finlayson [17] and Wilson et al. [38] for certain rheological fluids. Nevertheless, various types of nonlinear instability are present in these flows, and are a consequence of the nonNewtonian terms in the stress fields [30]. However, for a Reiner–Rivlin fluid in which time-derivatives of the stress tensor are not present, Graebel [11] found that the nonlinear viscous terms have a destabilizing influence, and this is consistent with the numerical results of Forbes [9]. Perhaps the most intriguing flows of viscoelastic fluids are those involving certain polymers, where even at low speeds, strong nonlinear instabilities may arise, resulting in *elastic turbulence* [20]. When polymers are dissolved in fluids, their presence may reduce the critical Reynolds number at which instability is observed, and the interaction has been referred to as "elasto-inertial turbulence" by Samanta et al. [29]. Flows having the appearance of fully developed turbulence have been measured experimentally at arbitrarily small Reynolds numbers, and are described by Larson [16] and Groisman and Steinberg [12].

The present paper follows, to some extent, the investigation begun by Forbes [9] of the turbulence properties of the Reiner–Rivlin equation. Here, the simplest of all viscous flows is studied, because it allows a deeper analysis. The flow in question is Couette flow [6], which is an exact solution both for the Navier–Stokes and the Reiner–Rivlin equations. It is a simple uni-directional shear flow with a linear velocity profile

https://doi.org/10.1017/S1446181115000176 Published online by Cambridge University Press

in the vertical $z$-coordinate. The governing equations are briefly reviewed in Section 2, and the linearized stability equations for small-amplitude perturbations are discussed in Section 3. This involves a classical eigenvalue analysis of a linearized system of equations equivalent to an Orr–Sommerfeld equation (see Drazin and Reid [6, p. 156]). Numerical results are presented that show how accounting for material nonlinearity may permit large numbers of eigenvalues to cross into the unstable zone $\mathrm{Im}\{\omega\} = \omega_I > 0$ more or less simultaneously, and at significantly lower Reynolds numbers than anticipated purely on the basis of Navier–Stokes theory. This confirms the results of Forbes [9], and likewise suggests that turbulence may thus be the result of material nonlinearity that causes the sudden appearance of high-dimensional chaos through quasi-periodicity and the Ruelle–Takens–Newhouse mechanism [34, p. 196]. The simpler nature of Couette flow also permits approximate stability zones to be computed in parameter space; some of these are illustrated in Section 3. Furthermore, when Reynolds number becomes infinite and only the nonlinear viscous terms are present, the eigenvalue distribution has an intriguing structure. Although this *elasto-inertial* limit may perhaps not be immediately relevant to turbulence in commonly experienced fluids, it is nevertheless important, because it reveals the role played by material nonlinearity more generally. In addition, it permits asymptotic validation of some features of the numerical results, in the case of Couette flow. This limit is therefore studied in Section 4. The paper concludes with a discussion in Section 5.

## 2. The governing equations

The details of this approach are given in the text by Aris [1] and reviewed at some length by Forbes [9], and so only a brief overview will be given here. A Cartesian coordinate system is present with axes represented as $(x_1, x_2, x_3) = (x, y, z)$, in which $x$ is the streamwise coordinate, $y$ points laterally and $z$ is directed vertically. The fluid velocity vector is denoted by the symbol $\mathbf{q}$ and its three components in Cartesian coordinates are $(q_1, q_2, q_3) = (u, v, w)$.

The fundamental equation in classical continuum mechanics is Cauchy's law

$$\frac{\partial \mathbf{q}}{\partial t} + (\mathbf{q} \cdot \nabla)\mathbf{q} = \mathbf{f} + \frac{1}{\rho} \operatorname{div} \mathbf{T}, \tag{2.1}$$

which expresses the conservation of linear momentum. Here, the fluid density is $\rho$, and since the fluid is taken to be incompressible, $\rho$ is a constant and, as a result, the law of conservation of mass may be expressed as

$$\operatorname{div} \mathbf{q} = 0. \tag{2.2}$$

The relation (2.1) is given in Aris [1, p. 102] and Mase [18, p. 128]. The symbol $\mathbf{f}$ denotes the body force vector per mass acting on the fluid, and $\mathbf{T}$ is the stress tensor.

In Navier–Stokes theory, the stress tensor $\mathbf{T}$ is assumed to depend *linearly* on the rate of strain tensor

$$\mathbf{D} = \tfrac{1}{2}(\nabla \mathbf{q} + \nabla \mathbf{q}^{\mathrm{T}}). \tag{2.3}$$

https://doi.org/10.1017/S1446181115000176 Published online by Cambridge University Press

Here, the notation $\nabla\mathbf{q}$ indicates a matrix of derivatives of the velocity vector components (the velocity gradient tensor in Mase [18, p. 112]), and $\nabla\mathbf{q}^{\mathrm{T}}$ is its transpose. If $p$ represents the pressure in the fluid, then the constitutive relation is taken to have the form

$$\mathbf{T} = -p\mathbf{I} + 2\mu\mathbf{D},$$

where $\mathbf{I}$ is the three-dimensional identity matrix and the constant $\mu$ is the usual dynamic viscosity of the fluid. This linear relationship between stress $\mathbf{T}$ and strain rate $\mathbf{D}$ in equation (2.3) is the Newtonian assumption, and it yields the familiar Navier–Stokes equation

$$\frac{\partial\mathbf{q}}{\partial t} + (\mathbf{q}\cdot\nabla)\mathbf{q} + \frac{1}{\rho}\nabla p = \mathbf{f} + \frac{\mu}{\rho}\nabla^2\mathbf{q}. \tag{2.4}$$

Reiner [24] and Rivlin [27], however, sought to generalize the description of the stress tensor $\mathbf{T}$ for a viscous fluid, to allow a general nonlinear analytic dependence on the strain rate tensor $\mathbf{D}$ in equation (2.3). It turns out that this may be achieved, without loss of generality, simply by including the *square* of the tensor $\mathbf{D}$ only, due to the Cayley–Hamilton theorem, and this is discussed further by Aris [1, Section 5.22] and Forbes [9]. The simplest form of this relationship now becomes

$$\mathbf{T} = -p\mathbf{I} + 2\mu\mathbf{D} + 2\tau\mathbf{D}^2$$

with a second (nonlinear) viscosity coefficient $\tau$. This gives rise to the simplest form

$$\frac{\partial\mathbf{q}}{\partial t} + (\mathbf{q}\cdot\nabla)\mathbf{q} + \frac{1}{\rho}\nabla p = \mathbf{f} + \frac{\mu}{\rho}\nabla^2\mathbf{q} + \frac{2\tau}{\rho}\,\mathrm{div}(\mathbf{D}^2) \tag{2.5}$$

of the Reiner–Rivlin equation. Forbes [9] showed that this equation (2.5) gives identical solutions for the velocity vector $\mathbf{q}$ as the Navier–Stokes equation (2.4) in two-dimensional flow, but with different pressures. However, the three-dimensional version of equation (2.5) possesses extra sources of vorticity, not available to the Navier–Stokes equation (2.4).

Now consider Couette flow of a viscous fluid between parallel horizontal impermeable plates located on the two surfaces $z = -H$, and $z = H$. The top plate has speed $-V$ in the horizontal $x$-direction, and the bottom plate moves with speed $V$, in the opposite direction to the top plate. This establishes the simple one-dimensional shear flow $u(z) = -(V/H)z$, in which the streamwise component of velocity has a linear profile with height $z$. The lateral and vertical velocity components are $v = 0$ and $w = 0$, respectively. The pressure $p$ for this flow can be taken to be zero throughout the fluid. The problem may be nondimensionalized using the length $H$ and speed $V$ as reference quantities and, as a result, there are now two important dimensionless parameters

$$R_e = \frac{\rho HV}{\mu} \quad \text{and} \quad F = \frac{\rho H^2}{\tau} \tag{2.6}$$

describing the flow. The first of these is the familiar Reynolds number $R_e$ that gives the inverse nondimensional viscosity. The second constant $F$ is the inverse of the

https://doi.org/10.1017/S1446181115000176 Published online by Cambridge University Press

coefficient of nonlinear viscosity, and measures the effect of material nonlinearity. In much of the rheological literature, this parameter $F$ is substituted with either the Weissenberg or Deborah number (see Poole [21]), but since those parameters are dependent on the Reynolds number, they are avoided here in favour of the constant $F$ in equation (2.6), as in Forbes [9].

## 3. Linear stability of plane Couette flow

The simple Couette flow velocity $(u, v, w) = (-z, 0, 0)$ in dimensionless variables is now subject to a perturbation $\epsilon(u_1, v_1, w_1)$, in which $\epsilon$ is an appropriately small dimensionless constant. The pressure $p$ is similarly assumed to be $\epsilon p_1$. Importantly, these perturbations must be fully three-dimensional, since the theorem proved by Forbes [9] shows that planar flows are indistinguishable from those obtained on the basis of the Navier–Stokes theory (2.4). These forms are now substituted into the Reiner–Rivlin equation (2.5), and terms retained only to first order in the small parameter $\epsilon$. In dimensionless form, it is now assumed that the perturbation functions can be represented as

$$\begin{aligned} u_1(x, y, z, t) &= \hat{u}_1(z) \exp(i[Kx + \Gamma y - \Omega t]) \\ v_1(x, y, z, t) &= \hat{v}_1(z) \exp(i[Kx + \Gamma y - \Omega t]) \\ w_1(x, y, z, t) &= \hat{w}_1(z) \exp(i[Kx + \Gamma y - \Omega t]) \\ p_1(x, y, z, t) &= \hat{p}_1(z) \exp(i[Kx + \Gamma y - \Omega t]). \end{aligned} \tag{3.1}$$

In these expressions, the dimensionless wavenumbers $K$ and $\Gamma$ in the streamwise and lateral directions, respectively, are real quantities, but the dimensionless frequency $\Omega = \omega(H/V)$ is in general a complex number. As discussed in Section 1, this parameter $\Omega$ (or its dimensional counterpart $\omega$) will be an eigenvalue of the stability problem to follow, and the perturbations (3.1) will be unstable if $\mathrm{Im}\{\Omega\} > 0$.

The continuity equation (2.2) allows the function $\hat{u}_1(z)$ in equations (3.1) to be eliminated at once from the formula

$$iK\hat{u}_1 + i\Gamma\hat{v}_1 + \frac{d\hat{w}_1}{dz} = 0. \tag{3.2}$$

Equations (3.1) are substituted into the linearized system that is derived from the Reiner–Rivlin equation (2.5), and the pressure function $\hat{p}_1(z)$ is eliminated by cross-differentiation. This leaves a system of two ordinary differential equations for the remaining two functions $\hat{v}_1(z)$ and $\hat{w}_1(z)$. The first equation is

$$\begin{aligned} &\frac{\Omega}{K}\left[i(K^2 + \Gamma^2)\hat{v}_1 + \Gamma\frac{d\hat{w}_1}{dz}\right] \\ &\quad = -i(K^2 + \Gamma^2)z\hat{v}_1 - \Gamma z\frac{d\hat{w}_1}{dz} + \Gamma\hat{w}_1 \\ &\qquad + \frac{1}{R_e K}\left[(K^2 + \Gamma^2)^2\hat{v}_1 - (K^2 + \Gamma^2)\left(\frac{d^2\hat{v}_1}{dz^2} + i\Gamma\frac{d\hat{w}_1}{dz}\right) + i\Gamma\frac{d^3\hat{w}_1}{dz^3}\right] \\ &\qquad + \frac{1}{2F}\left[(K^2 + \Gamma^2)\left(2i\frac{d\hat{v}_1}{dz} + \Gamma\hat{w}_1\right) + \Gamma\frac{d^2\hat{w}_1}{dz^2}\right] \end{aligned} \tag{3.3}$$

https://doi.org/10.1017/S1446181115000176 Published online by Cambridge University Press

and the second equation is

$$\Omega\Big[\Gamma\hat{w}_1 + i\frac{d\hat{v}_1}{dz}\Big] = -K\Gamma z\hat{w}_1 - iK\hat{v}_1 - iKz\frac{d\hat{v}_1}{dz} + \frac{1}{R_e}\Big[(K^2+\Gamma^2)\Big(\frac{d\hat{v}_1}{dz} - i\Gamma\hat{w}_1\Big) + i\Gamma\frac{d^2\hat{w}_1}{dz^2} - \frac{d^3\hat{v}_1}{dz^3}\Big] + \frac{1}{2KF}\Big[-i\Gamma^2(K^2+\Gamma^2)\hat{v}_1 + \Gamma(K^2-\Gamma^2)\frac{d\hat{w}_1}{dz} + i(\Gamma^2+2K^2)\frac{d^2\hat{v}_1}{dz^2} + \Gamma\frac{d^3\hat{w}_1}{dz^3}\Big]. \tag{3.4}$$

These two equations are to be solved subject to the no-slip boundary condition on the two plates at dimensionless heights $z = \pm 1$. In view of equation (3.2), the appropriate conditions for the two stability equations (3.3), (3.4) are therefore

$$\hat{v}_1 = \hat{w}_1 = \frac{d\hat{w}_1}{dz} = 0 \quad \text{on } z = \pm 1. \tag{3.5}$$

A solution is sought to the system (3.3)–(3.5) using a spectral representation. The two functions $\hat{v}_1$ and $\hat{w}_1$ are expressed as

$$\hat{v}_1(z) = \sum_{n=1}^{\infty} A_n\phi_n(z), \qquad \hat{w}_1(z) = \sum_{n=1}^{\infty} B_n\psi_n(z) \tag{3.6}$$

with basis functions

$$\phi_n(z) = \sin\Big(\frac{n}{2}\pi(z+1)\Big)$$
$$\psi_n(z) = \cos\Big(\frac{n}{2}\pi(z+1)\Big) - \cos\Big(\frac{n+2}{2}\pi(z+1)\Big) \tag{3.7}$$

chosen, so that the expressions (3.6) satisfy the boundary conditions (3.5) identically. These representations (3.6) are substituted into the two equations (3.3) and (3.4). The first equation (3.3) is then multiplied by the basis functions $\phi_k(z)$ and integrated over the domain $-1 < z < 1$. The second equation (3.4) can result in some ill-conditioned systems, and requires care. In an earlier version of this work, it was multiplied by functions $\psi_k(z)$, $k = 1, 2, \ldots$, and similarly integrated, but this can result in a spurious pair of eigenvalues $\Omega$ lying on the imaginary axis, and these move further away from the origin as the number of modes is increased. A similar difficulty has been noted by Valério et al. [36], and here the difficulty becomes more pronounced for lower wavenumbers $K$ and $\Gamma$. To overcome this ill-conditioning, equation (3.4) has been multiplied simply by test functions $\cos((k\pi/2)(z+1))$, $k = 1, 2, \ldots$, and integrated over its domain $-1 < z < 1$. This eliminates the problem of the false purely imaginary eigenvalues of magnitude that increases with the number of modes. Nevertheless, some ill-conditioning is still present, and for a very large $N$, a pair of spurious eigenvalues may still be produced: however, they have finite and negative imaginary parts, with large real parts of opposite sign, and so they do not affect the stability verdict.

https://doi.org/10.1017/S1446181115000176 Published online by Cambridge University Press

Because of the relative simplicity of Couette flow, all the resulting quadratures are evaluated exactly in closed form, so as to maintain accuracy. After a considerable amount of calculation, a system of linear algebraic equations is obtained, involving the Fourier coefficients $A_n$ and $B_n$. For numerical purposes, the infinite series (3.6) are truncated to some finite number of $N$ modes, and this results in a generalized eigenvalue problem of the form

$$\begin{bmatrix} \mathbf{P}^{(1A)} & \mathbf{P}^{(1B)} \\ \mathbf{P}^{(2A)} & \mathbf{P}^{(2B)} \end{bmatrix} \begin{bmatrix} \mathbf{A} \\ \mathbf{B} \end{bmatrix} = \Omega \begin{bmatrix} \mathbf{Q}^{(1A)} & \mathbf{Q}^{(1B)} \\ \mathbf{Q}^{(2A)} & \mathbf{Q}^{(2B)} \end{bmatrix} \begin{bmatrix} \mathbf{A} \\ \mathbf{B} \end{bmatrix}. \tag{3.8}$$

Here, the eight quantities $\mathbf{P}^{(1A)}, \ldots, \mathbf{Q}^{(2B)}$ are all $N \times N$ block matrices, and $[\mathbf{A}\,\mathbf{B}]^{\mathrm{T}}$ is a $2N \times 1$ vector containing the coefficients in the series in equation (3.6). For completeness and ease of reproducibility, the full form of (3.8) is given in the Appendix. This system is solved for the eigenvalues $\Omega$ using the *MATLAB* routine `eig`, which is an implementation of the QR algorithm. In fact, it is found that slightly more symmetrical results are achieved by creating the single matrix $\mathbf{Q}^{-1}\mathbf{P}$ using Gaussian elimination and then using the QR method to determine its eigenvalues directly. In many of the results to be presented here, the system (3.8) has been solved with $N = 151$ modes, so that a generalized eigenvalue problem of size $300 \times 300$ is produced. The code runs in only a few minutes on a standard laptop computer. The execution time increases significantly as more modes are used, and some such examples will be discussed in order to establish the convergence of the method.

Figure 1 presents the eigenvalue distribution in the complex $\Omega$-plane for wavenumbers $K = \Gamma = 80$ and Reynolds number $R_e = 4000$. This diagram affords a direct comparison between the result for pure Navier–Stokes theory, shown in Figure 1(a), and the predictions of Reiner–Rivlin theory in Figure 1(b). The classical Navier–Stokes result in (a) is obtained from the algorithm (3.8) simply by specifying that $1/F = 0$ in the code. Clearly, all the eigenvalues $\Omega$ have negative imaginary part, and so the perturbations (3.1) must decay as time increases and, as a result, the original Couette flow is predicted to be stable, as expected. On the other hand, the result in (b) for the Reiner–Rivlin case with $F = 500$ possesses a very large number of eigenvalues all with positive imaginary part at the approximate value $\mathrm{Im}\{\Omega\} \approx 30$. This is clearly a solution for which the perturbations (3.1) will grow exponentially with time, and so the base Couette flow will now be unstable. Furthermore, since the real parts are not integer multiples of one another, the linearized solution will contain a superposition of a large number of growing modes of frequencies of irrational multiples of each other, and thus would constitute an unstable quasi-periodic orbit of very high dimension. Forbes [9] argued that nonlinear effects in the full Reiner–Rivlin equation (2.5) would then trigger a bifurcation to high-dimensional chaos, and identified this as the explanation of fluid turbulence. The spectra shown in Figures 1(a) and (b) appear to contain isolated eigenvalues as well as continuous portions, although this cannot be confirmed purely on the basis of numerical results. Nevertheless, Valério et al. [36], in their analysis of the stability of viscoelastic flows, have presented results

https://doi.org/10.1017/S1446181115000176 Published online by Cambridge University Press

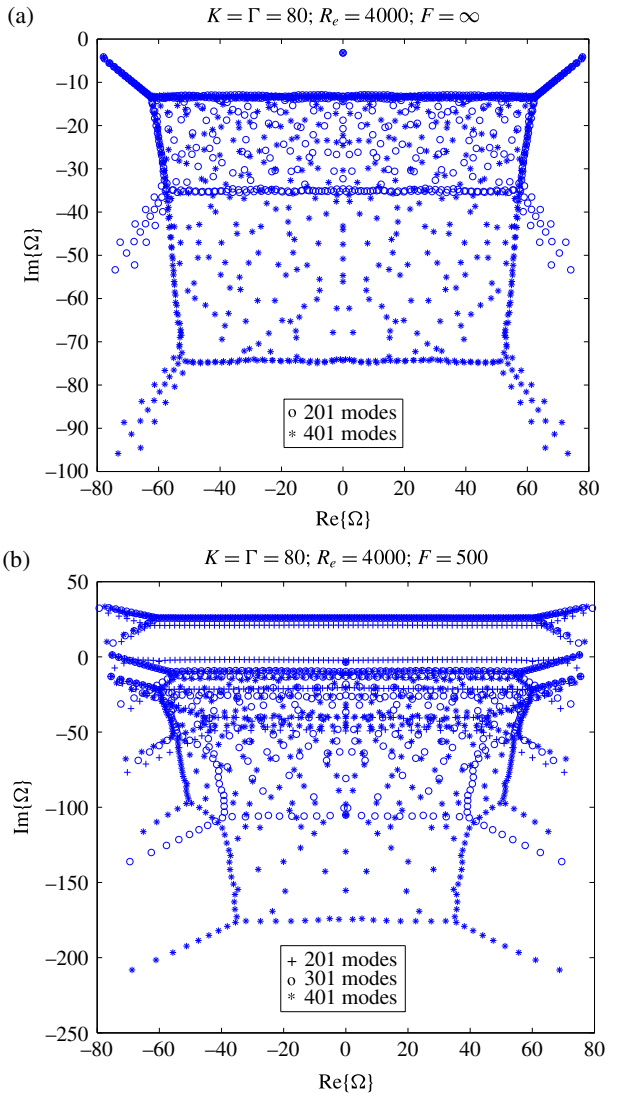


FIGURE 1. A comparison of the eigenvalue distribution for plane Couette flow, for (a) the Navier–Stokes system with $F = \infty$ and (b) the Reiner–Rivlin case with $F = 500$. The two dimensionless wavenumbers are $K = \Gamma = 80$ and the Reynolds number is $R_e = 4000$. Different numbers of modes are used in each case, to analyze convergence.

at least qualitatively similar to those in Figure 1(b) and discussed continuous spectra in those flows.

Figure 1 also permits an analysis of the convergence of the calculation of the eigenvalues $\Omega$ with increasing number of modes $N$. For the pure Navier–Stokes spectrum presented in Figure 1(a), results are shown with 201 and 401 modes

https://doi.org/10.1017/S1446181115000176 Published online by Cambridge University Press

which demonstrate features that have been observed consistently throughout this study. As more modes are included, there appear more eigenvalues with very large negative imaginary parts. There seems to be fairly little consistency in most of those eigenvalues, and so it is reasonable to suggest that they may not be genuinely part of the spectrum of the exact linear differential equations (3.3) and (3.4). In any case, those modes would decay so rapidly that they would have little effect on the numerical solution. However, there is a high degree of convergence on the approximately U-shaped structure at the top of Figure 1(a). The uppermost eigenvalues (the ones that determine the stability) have converged at least to graphical accuracy (about three significant figures), although convergence is somewhat slower near the approximately horizontal section. This is again consistent with the work of Valério et al. [36] who observed slower convergence close to continuous portions of the spectrum. Similar comments apply for the unstable Couette flow in the Reiner–Rivlin case illustrated in Figure 1(b). There, the results with $N = 201$ modes for the apparently continuous section at the top of that figure are still not quite converged, but the two sets of values with $N = 301$ and $N = 401$ modes are almost indistinguishable in that portion of the diagram. Lower down on that figure, there are also some isolated eigenvalues which are highly converged and some apparently continuous portions which likewise may be genuinely part of the spectrum, although there are also many eigenvalues with very large negative imaginary parts that appear not to be genuine. However, they are not of primary concern in this discussion of turbulence and its possible causes.

The algorithm (3.8) has been run for a large set of values of the Reynolds number $R_e$ and nonlinear viscosity coefficient $F$, for a variety of streamwise and transverse wavenumbers $K$ and $\Gamma$. Of particular interest has been the critical value of the Reynolds number $R_e$ at which stable Couette flow first becomes unstable in flow described by the Reiner–Rivlin equation (2.5), since this may correspond to the transition to turbulence in this flow. Recall that in Navier–Stokes theory, this simple Couette shear flow apparently *never* loses its stability in the linearized (small disturbance) case [6]. This theory is recovered from the Reiner–Rivlin equation (2.5) only in the limit $F \to \infty$ at which the nonlinear viscous terms disappear entirely.

It turns out that, for most of the wavenumbers $K$ and $\Gamma$ investigated, there are *two* values of the Reynolds number that are of interest in the transition to unstable flow. At the lower Reynolds number, a single pair of eigenvalues crosses into the unstable zone $\mathrm{Im}\{\Omega\} > 0$, and this is the first point of instability. However, at a somewhat higher Reynolds number, a very large number of eigenvalues cross this boundary almost simultaneously: it is suggested here that this may be the true trigger of turbulent behaviour in the full nonlinear system, since this event produces a linear solution of high-dimensional quasi-periodic behaviour, which is structurally unstable in the nonlinear case and collapses into high-dimensional chaos by the Ruelle–Takens–Newhouse mechanism [34, p. 196]. The difference between these two critical Reynolds numbers depends particularly sensitively on the value of the streamwise wavenumber $K$.

This is illustrated in Figure 2 for streamwise and transverse wavenumbers $K = \Gamma = 100$. For a variety of different values of $F$ (on the vertical axis), numerical results were

https://doi.org/10.1017/S1446181115000176 Published online by Cambridge University Press

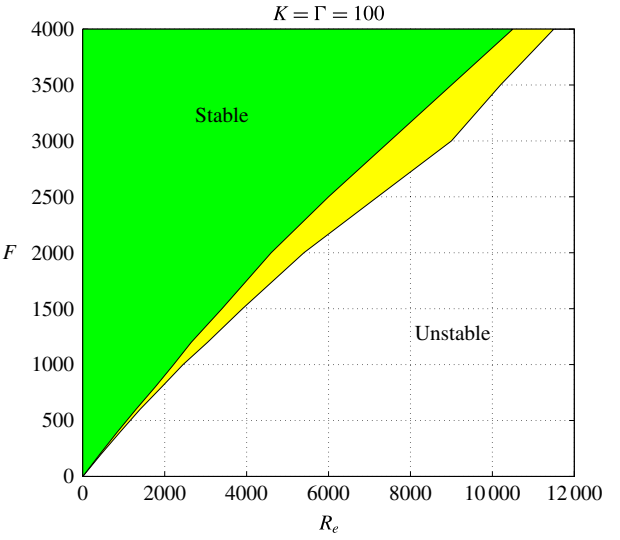


FIGURE 2. Stability region for plane Couette flow, dependent on the two (inverse) viscosity parameters $R_e$ and $F$. The two dimensionless wavenumbers are $K = \Gamma = 100$. The darker (green) region represents unconditional stability, the middle (yellow) zone corresponds to instability of only a single pair of modes, and the region to the right contains solutions with a high-dimensional unstable quasi-periodic orbit, which in the nonlinear equations would correspond to turbulence. (Colour available online.)

obtained for many different values of Reynolds number $R_e$ (on the horizontal axis), and an estimate was made by eye of the values at which a single eigenvalue pair crossed into the unstable zone, and then when an ensemble of eigenvalues crossed into this region in the complex plane, at a slightly higher Reynolds number. Necessarily, these judgements are somewhat subjective, particularly in the latter case, and this is why the stability boundaries in Figure 2 are a little irregular.

The Couette flow is unconditionally stable in a linearized theory, for low Reynolds numbers in the darker shaded region (green online in Figure 2) to the left of the diagram. In this zone, every eigenvalue has a negative imaginary part. Notice that as $F \to \infty$ and the Navier–Stokes limit is recovered, this unconditionally stable zone apparently extends out to an arbitrarily large Reynolds number. The first boundary, between the darker (green online) and lighter (yellow online) regions is the value of Reynolds number at which a single eigenvalue pair first develops a positive imaginary part, $\mathrm{Im}\{\Omega\} > 0$. In the lighter (yellow) zone between the two boundaries, the flow is thus unstable, but only to one single mode. However, the second boundary on the border of the region marked "unstable" is an estimate of the Reynolds number at which an entire line of eigenvalues crosses into the unstable zone, so that high-dimensional quasi-periodic behaviour ensues. This is possibly the border of greater interest, since Reynolds numbers $R_e$ larger than about this value would give solutions that would be turbulent in the fully nonlinear theory.

Figure 3 shows the distribution of eigenvalues $\Omega$ in the complex plane, corresponding to a horizontal slice through Figure 2 at the inverse nonlinear viscosity

https://doi.org/10.1017/S1446181115000176 Published online by Cambridge University Press

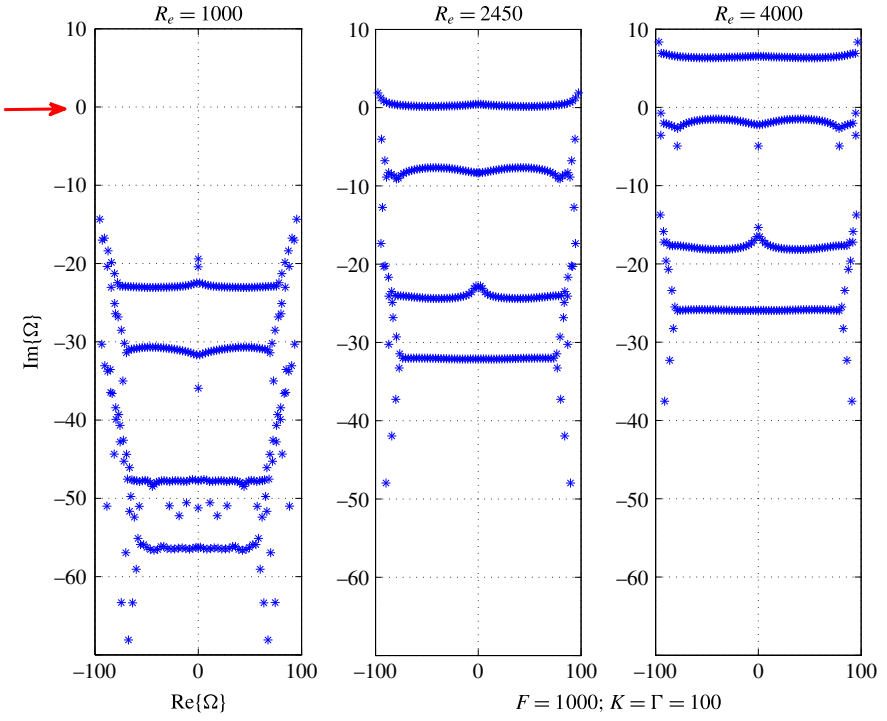


FIGURE 3. Distribution of eigenvalues in the complex plane for nonlinear viscosity coefficient $F = 1000$. Results are shown for the three values of Reynolds number $R_e = 1000$, $R_e = 2450$ and $R_e = 4000$. The two dimensionless wavenumbers are $K = \Gamma = 100$. The (red) arrow shows the boundary between the stable and unstable zones for all three diagrams.

parameter $F = 1000$. As previously, the two wavenumbers for this case are $K = \Gamma = 100$. The (red) arrow at the left of the diagram marks the level at which $\mathrm{Im}\{\Omega\} = 0$, and so eigenvalues below this line correspond to stable modes, while those above the line represent unstable modes that grow exponentially with time in the linearized theory.

In the first diagram on the left of Figure 3, the Reynolds number has the value $R_e = 1000$, and this is well within the darker (green) stable zone in Figure 2. This corresponds to a solution that is unconditionally stable, which is evident from the diagram, since all the eigenvalues lie well within the stable zone $\mathrm{Im}\{\Omega\} < 0$.

The middle diagram in Figure 3 has Reynolds number $R_e = 2450$. It lies on the second boundary to the right of Figure 2, and so has been identified here as being at about the point of transition to turbulent flow. Observe that, although one or two eigenvalues had already crossed into the unstable zone at a slightly lower Reynolds number (about $R_e = 2220$), at $R_e = 2450$ an entire line of eigenvalues crosses into the unstable section $\mathrm{Im}\{\Omega\} > 0$ of the complex plane. In the final diagram on the right-hand side of Figure 3, with Reynolds number $R_e = 4000$, that line of eigenvalues has

https://doi.org/10.1017/S1446181115000176 Published online by Cambridge University Press

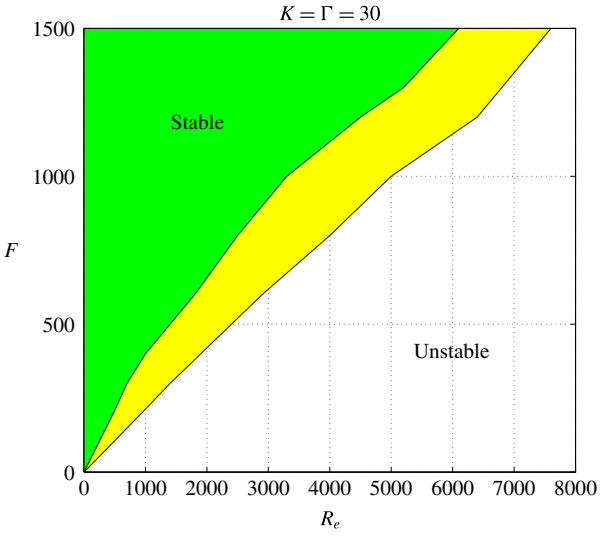


FIGURE 4. Stability region for plane Couette flow, dependent on the two (inverse) viscosity parameters $R_e$ and $F$. The two dimensionless wavenumbers are $K = \Gamma = 30$. The darker (green) region represents unconditional stability, and the region to the right contains solutions with only a single unstable mode. (Colour available online.)

now moved strongly into the unstable zone. In linearized theory, the large number of unstable modes it creates, with their arbitrary different frequencies, would generate a complicated quasi-periodic orbit; nonlinear effects would then cause a rapid transition to a high-dimensional chaotic attractor. This is the structure that is suggested by Forbes [9] to be the cause of true fluid turbulence.

Similar results to those shown in Figure 2 are obtained at other values of the wavenumbers. Another such case is illustrated in Figure 4, for the lower wavenumbers $K = \Gamma = 30$. Again, there is a darker shaded (green online) region to the left, in which all the eigenvalues have negative imaginary parts, so that the underlying Couette flow is stable in that parameter region. There is again an intermediate zone (yellow online) in which the flow is unstable to a single pair of eigenvalues, and the clear region to the right of the diagram is the zone in which a large number of eigenvalues exist with positive imaginary parts and real parts that are not rational multiples of each other. Turbulence is anticipated to occur in that parameter space. The borders between these three regions have again been estimated by eye from a large number of computer runs, and so are a little irregular.

A horizontal slice through the stability diagram in Figure 4 with $K = \Gamma = 30$ is again depicted in Figure 5, at the value $F = 1000$ of the inverse nonlinear viscosity coefficient. Eigenvalue distributions are shown for the three different Reynolds numbers $R_e = 500$, 5000 and 8000. A similar pattern of behaviour is observed, as for the higher wavenumbers $K = \Gamma = 100$ presented in Figure 3. The first picture on the left side of Figure 5 is for a solution with Reynolds number $R_e = 500$, and all its

https://doi.org/10.1017/S1446181115000176 Published online by Cambridge University Press

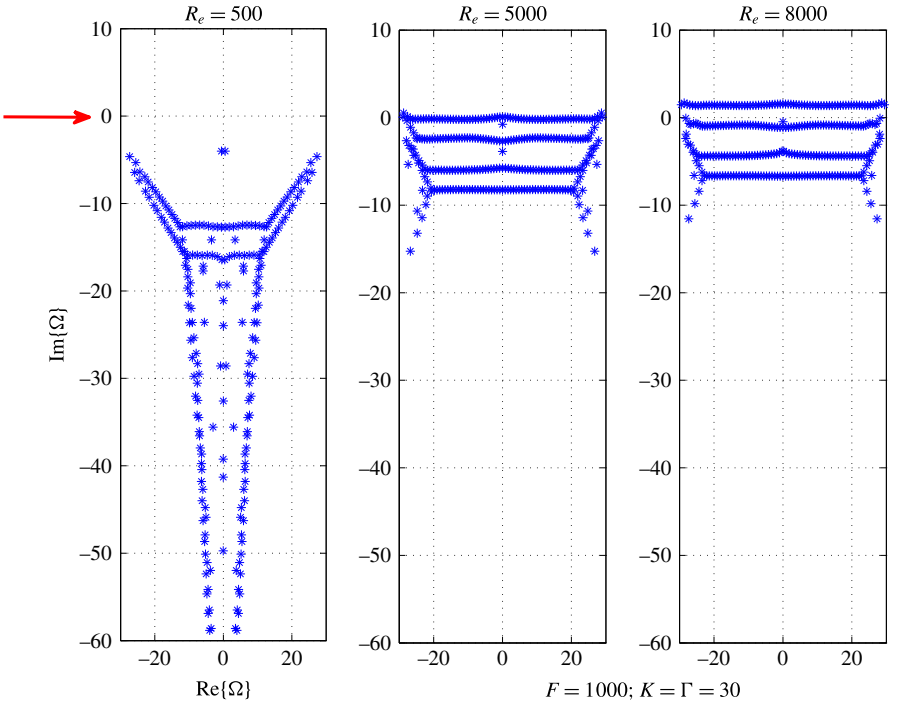


FIGURE 5. Distribution of eigenvalues in the complex plane for nonlinear viscosity coefficient $F = 1000$. Results are shown for the three values of Reynolds number $R_e = 500$, $R_e = 5000$ and $R_e = 8000$. The two dimensionless wavenumbers are $K = \Gamma = 30$. The (red) arrow shows the boundary between the stable and unstable zones for all three diagrams.

eigenvalues lie well within the region of stability, in which the imaginary part of each eigenvalue $\Omega$ is negative. In the central frame, for which $R_e = 5000$, the approximately horizontal line of eigenvalues has moved upwards and is poised to cross into the unstable zone $\mathrm{Im}\{\Omega\} > 0$. The final diagram on the right-hand side of Figure 5 now represents an unstable solution, since the line of eigenvalues has now crossed into the unstable zone, producing a high-dimensional quasi-periodic solution in the linearized theory and therefore a chaotic solution of high dimension when nonlinear effects are taken into account.

In a practical experiment, it is unlikely that the perturbation to Couette flow would consist simply of a single pair of wavenumbers $K$, $\Gamma$ as discussed in this section. Instead, it is to be expected that an arbitrary perturbation would involve a large number of such solutions, and so the actual distribution of eigenvalues would no doubt be a complicated superposition of many results like those shown in Figures 3 and 5. Thus, even in linearized theory before nonlinear effects are taken into account, an unstable solution in the Reiner–Rivlin scenario would represent a structure of remarkable complexity.

https://doi.org/10.1017/S1446181115000176 Published online by Cambridge University Press

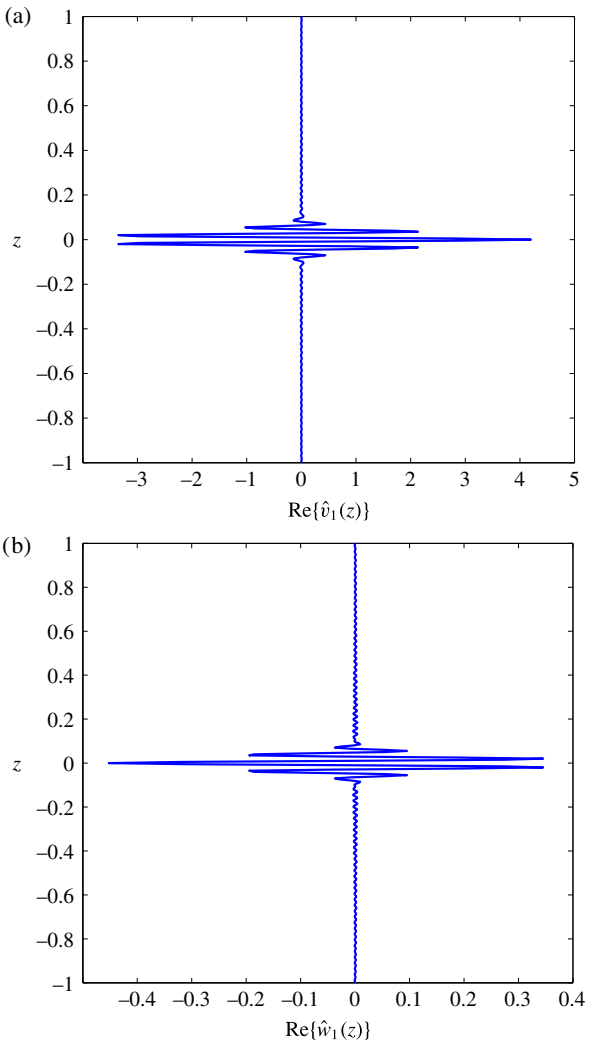


FIGURE 6. The eigenvectors (a) $\hat{v}_1(z)$ and (b) $\hat{w}_1(z)$ corresponding to the single eigenvalue $\Omega = 0 + 0.0379i$, for Reynolds number $R_e = 5000$ and nonlinear viscosity coefficient $F = 1000$. The two dimensionless wavenumbers are $K = \Gamma = 30$.

The eigenfunction for a mode that is about to become unstable is considered in Figure 6. This is taken from the central panel in Figure 5 for the eigenvalue in the centre of the (possibly continuous) line that is about to cross into the unstable zone, and is the one located purely on the imaginary axis. The eigenvalue in question has the value $\Omega = 0 + 0.0379i$ and thus represents a mode that is marginally unstable. The Reynolds number is $R_e = 5000$ and the other parameters are as in Figure 5. The coefficients $A_n$ and $B_n$ that comprise the eigenvector in equation (3.8) for that particular

https://doi.org/10.1017/S1446181115000176 Published online by Cambridge University Press

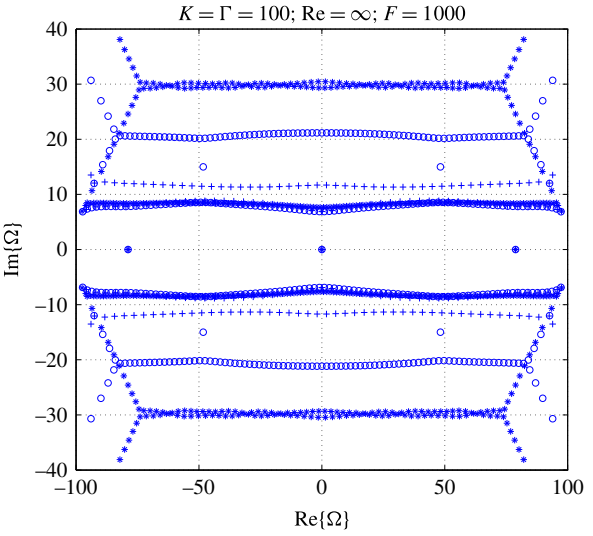


FIGURE 7. Distribution of eigenvalues in the complex plane for nonlinear viscosity coefficient $F = 1000$. Results are shown for infinite Reynolds number $R_e = \infty$. The two dimensionless wavenumbers are $K = \Gamma = 100$. A convergence analysis is included, using $N = 101$ modes (+), $N = 201$ modes (o) and $N = 301$ modes (*).

eigenvalue are identified from the solution algorithm, and then the functions $\hat{v}_1$ and $\hat{w}_1$ are reconstructed from the spectral forms (3.6). They are illustrated in Figure 6 over the domain $-1 < z < 1$ between the plates. In each variable, the perturbation mode consists of a peaked disturbance localized near the centre of the channel. Qualitatively similar results for more complex viscoelastic fluids were also obtained by Valério et al. [36].

## 4. Extended results for infinite Reynolds number

Although it is possibly not immediately applicable to the study of turbulence in fluids that are commonly encountered, it is nevertheless of value to study the extreme case of infinite Reynolds number, in which the only contribution to viscosity is through the nonlinear nonNewtonian terms. This is achieved in the present algorithm simply by setting the parameter $1/R_e$ to zero, and so represents the "elasto-inertial" situation [29].

**4.1. Numerical results** The distribution of eigenvalues in the complex $\Omega$-plane for a solution with infinite Reynolds number $R_e = \infty$ is displayed in Figure 7. Here, the wavenumbers are $K = \Gamma = 100$ and the nonlinear viscosity coefficient is $F = 1000$. There is a single eigenvalue $\Omega = 0 + i0$ in the centre of the figure and, interestingly, the distribution of eigenvalues at this value of $F$ appears to be symmetrical both about the vertical line $\mathrm{Re}\{\Omega\} = 0$ and the horizontal line $\mathrm{Im}\{\Omega\} = 0$, giving apparent four-fold symmetry. In this diagram, results have been shown for 101, 201 and 301 modes, as a further check on the convergence of the eigenvalues. There are two nearly-horizontal lines of eigenvalues at about $\mathrm{Im}\{\Omega\} \approx \pm 8$, for which convergence with 201 and 301

https://doi.org/10.1017/S1446181115000176 Published online by Cambridge University Press

modes is reasonable. There is a high degree of convergence for the isolated eigenvalues shown on the real axis. However, there is no consistency in the remaining eigenvalues outside this central region, with more being added further out as the number of modes $N$ is increased. Therefore, these are unlikely to be genuine solution modes, although the central portion $-10 < \mathrm{Im}\{\Omega\} < 10$ is nevertheless reliable.

**4.2. Asymptotic results** A useful approximate check on the validity of results such as those shown in Figure 7 is possible for the case $1/R_e = 0$, by supposing that the second viscosity coefficient $1/F$ is large. In that case, equations (3.3), (3.4) reduce to the approximate set

$$\frac{\Omega}{K}\left[i(K^2+\Gamma^2)\hat{v}_1 + \Gamma\frac{d\hat{w}_1}{dz}\right] \approx \frac{1}{2F}\left[(K^2+\Gamma^2)\left(2i\frac{d\hat{v}_1}{dz} + \Gamma\hat{w}_1\right) + \Gamma\frac{d^2\hat{w}_1}{dz^2}\right], \tag{4.1}$$

and

$$\Omega\left[\Gamma\hat{w}_1 + i\frac{d\hat{v}_1}{dz}\right] \approx \frac{1}{2KF}\left[-i\Gamma^2(K^2+\Gamma^2)\hat{v}_1 + \Gamma(K^2-\Gamma^2)\frac{d\hat{w}_1}{dz} + i(\Gamma^2+2K^2)\frac{d^2\hat{v}_1}{dz^2} + \Gamma\frac{d^3\hat{w}_1}{dz^3}\right]. \tag{4.2}$$

As these are now constant-coefficient linear differential equations, they permit an exponential solution, in which both functions $\hat{v}_1$ and $\hat{w}_1$ contain a factor $\exp(\lambda z)$. After some considerable algebra, equations (4.1), (4.2) are combined to yield a quartic equation for the exponent $\lambda$. This complicated expression may be shown to reduce to the form

$$(\lambda^2 - \xi^2)[\Gamma^2\lambda^2 + 4(\Omega F)K\lambda - \{4(\Omega F)^2 + \xi^2\Gamma^2\}] = 0, \tag{4.3}$$

where $\xi = \sqrt{K^2+\Gamma^2}$ has been defined for convenience. The four roots of this quartic are written as

$$\pm\xi, \quad -\alpha+\beta, \quad -\alpha-\beta, \tag{4.4}$$

where the two parameters

$$\alpha = \frac{2(\Omega F)K}{\Gamma^2}; \quad \beta = \frac{\xi}{\Gamma^2}\sqrt{4(\Omega F)^2+\Gamma^4} \tag{4.5}$$

involve the unknown eigenvalue $\Omega$.

These four roots (4.4) of the quartic (4.3) show that the asymptotic form for the function $\hat{w}_1$ is

$$\hat{w}_1(z) = C_1\cosh(\xi(z+1)) + C_2\sinh(\xi(z+1)) + e^{-\alpha z}[C_3\cosh(\beta(z+1)) + C_4\sinh(\beta(z+1))], \tag{4.6}$$

where the four constants $C_1, \ldots, C_4$ are as yet unknown. The fluid is required to satisfy the no-slip boundary conditions on the two plates at $z = \pm 1$, and so the function $\hat{w}_1$ in

https://doi.org/10.1017/S1446181115000176 Published online by Cambridge University Press

equation (4.6), and its first derivative, must both be zero there as in equation (3.5). At the lower plate $z = -1$. This immediately gives the relations

$$C_1 = -e^{\alpha} C_3,$$
$$C_2 = \frac{1}{\xi} e^{\alpha} (\alpha C_3 - \beta C_4).$$

The two conditions are similarly applied at the upper plate $z = 1$. The constant $C_4$ may be eliminated in favour of $C_3$ which must remain arbitrary to avoid a trivial solution. Consequently, the dispersion relation

$$-2\beta \cosh(2\alpha) + \sinh(2\beta) \sinh(2\xi) \left[ \frac{(\alpha^2 - \beta^2)}{\xi} - \xi \right] + 2\beta \cosh(2\beta) \cosh(2\xi) = 0 \quad (4.7)$$

is obtained after further substantial algebra.

The dispersion relation (4.7) is a difficult nonlinear transcendental equation for the eigenvalue $\Omega$, when the relations (4.5) are taken into account. Consequently, solutions are extremely difficult to obtain. Nevertheless, by inspection, two possibilities present themselves. The first occurs when $\alpha = 0$ and $\beta = \xi$, and the second results from the choice, $\beta = 0$. These give the two sets of eigenvalues

$$\Omega = 0 \quad \text{and} \quad \Omega = \pm i \frac{\Gamma^2}{2F}. \quad (4.8)$$

Thus, in this asymptotic limit, one eigenvalue is always zero and the others occur as a complex conjugate pair. This shows that there is always an eigenvalue with $\mathrm{Im}\{\Omega\} > 0$ so that the effect of large nonlinear viscosity coefficient $1/F$ is always to destabilize the flow. This is further confirmed by observing that equation (4.7) remains satisfied if $\Omega$ is replaced with $-\Omega$. Thus the complex plane of the eigenvalues is invariant to a rotation of 180 degrees about the origin.

The eigenvalue distribution is shown in Figure 8 for infinite Reynolds number $R_e = \infty$ and a reasonably large value $F = 100$ for the inverse nonlinear viscosity coefficient. These results were obtained from the generalized eigenvalue problem (3.8) as previously. The eigenvalue distribution exhibits the four-fold symmetry observed in Figure 7, although again it is only the central portion containing the two horizontal lines of eigenvalues that can be considered as part of the genuine spectrum of the differential equation system. Nevertheless, the flow pattern corresponding to the situation depicted in Figure 8 would clearly possess unstable modes at many different frequencies, and nonlinear effects would result in a bifurcation to high-dimensional chaos. Such a solution would, therefore, represent an example of "elasto-inertial turbulence" as discussed by Samanta et al. [29].

The results of the approximate asymptotic solution (4.8) are also drawn on Figure 8 with three small circles (red online). As in Figure 7, there is again an eigenvalue at the origin of Figure 8, and this agrees entirely with the result $\Omega = 0$ in the asymptotic solution (4.8). The complex conjugate pair $\Omega = \pm 50i$ in the asymptotic prediction (4.8) for these parameter values is also indicated on the diagram, and agrees moderately well with the full numerical results. It is found that this agreement improves as $F$ is reduced, as anticipated. A very similar outcome is achieved when $F$ is made negative.

https://doi.org/10.1017/S1446181115000176 Published online by Cambridge University Press

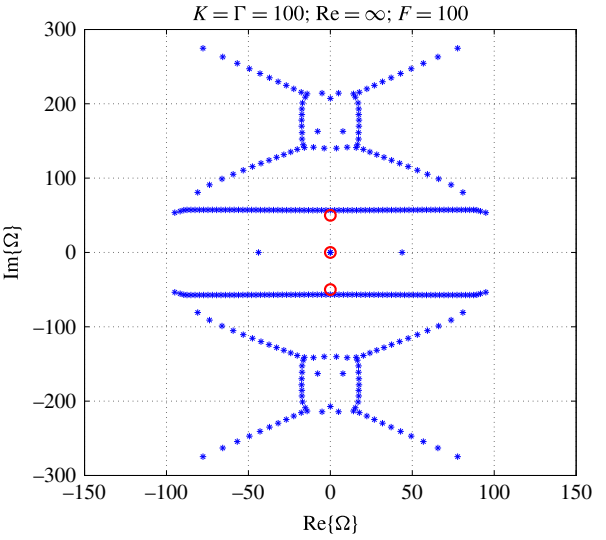


FIGURE 8. Distribution of eigenvalues in the complex plane for nonlinear viscosity coefficient $F = 100$. Results are shown for infinite Reynolds number $R_e = \infty$. The two dimensionless wavenumbers are $K = \Gamma = 100$. The three (red) circles are the results of the asymptotic solution in equation (4.8).

## 5. Conclusion

The stability of plane Couette flow to small perturbations has been studied here for a fluid that may possess some degree of material nonlinearity. The reason for this is to explore the proposition advanced by Forbes [9] that small amounts of nonlinear viscosity coupled with moderately high wavenumber perturbations can produce instability of a rather complicated form, even when the classical Navier–Stokes equations of viscous flow predict this flow to be stable. In these cases, it is found that there is a critical Reynolds number $R_e$ at which a large number of eigenmodes of the flow become unstable almost simultaneously, and at frequencies that are not integer multiples of one another. In linear, small-perturbation theory this would result in high-dimensional, quasi-periodic behaviour in time, but nonlinear effects would cause a bifurcation to a chaotic attractor of high dimension. Forbes [9] identified this as an explanation for the transition from laminar to turbulent flow in plane Poiseuille flow. Similar behaviour has been confirmed here for the simpler Couette flow, in which the velocity profile is linear. The Navier–Stokes equations (2.4) predict that Couette flow is unconditionally stable to small perturbations at any Reynolds number [6], but this is not confirmed by experiment. However, the Reiner–Rivlin equations (2.5) show that predictions of critical Reynolds number, commensurate with experimental findings, could occur at appropriate wavenumbers $K$, $\Gamma$ and nonlinear viscosity $1/F$.

The numerical solution of this linearized problem has been accomplished using an accurate spectral method, based on the representations in equations (3.6), (3.7),

https://doi.org/10.1017/S1446181115000176 Published online by Cambridge University Press

which are in fact slightly more general than those in Forbes [9] since they are not restricted to symmetric modes only. The simpler structure of the Orr–Sommerfeld type equations arising from Couette flow precludes a consideration of only the symmetric modes, unlike the situation in the slightly more complicated Poiseuille flow studied in [9]. Paradoxically, this makes the numerical determination of the eigenvalues somewhat more difficult, since the nonorthogonal basis functions (3.7) introduce a degree of ill-conditioning. This is discussed by Frederiksen [10] in a related stability problem arising in meteorology, and in some detail for viscoelastic fluids by Reddy et al. [23] and Valério et al. [36]. The simple decomposition algorithm presented here is sufficient to contain the effects of this ill-conditioning, and convergence to the key eigenvalues of interest has been demonstrated.

The results presented here give a reasonably consistent view of how turbulence may arise in Couette flow, and of its underlying mathematical structure. At high Reynolds numbers, the distribution of eigenvalues is almost symmetrical about the real axis in the complex eigenvalue plane. This means that even small amounts of nonlinear viscosity $\tau$ cause a destabilization of the flow, with a large number of unstable modes over a range of different frequencies. This structure would be encountered reasonably abruptly as Reynolds number is increased beyond a certain value, and thus would result in turbulent behaviour almost immediately. The effect of the usual (linear) dynamic viscosity coefficient $\mu$ is to stabilize the flow, and this is accomplished mathematically essentially by moving the entire pattern of eigenvalues downward toward the region of negative imaginary part. This behaviour was evident in Figures 3 and 5. The simpler structure of Couette flow permitted this understanding of the structure to be confirmed by an asymptotic solution valid at high Reynolds numbers.

It may, therefore, be the case that fluid turbulence is indeed a manifestation of weakly nonNewtonian effects [9] with similar underlying physics and mathematical structure as the exotic "elasto-inertial turbulence" phenomena encountered in rheological flows of polymer fluids, such as those shown by Larson [16]. This seems worthy of further theoretical and experimental investigation. In addition, as discussed in [9], a method for the determination of the nonlinear viscosity parameter $F$ for common fluids is also suggested by this work, since uni-directional and planar flows calculated using the Reiner–Rivlin equation (2.5) have identical velocity patterns to those of Navier–Stokes theory, but different fluid pressures. Consequently, careful experimental measurements of wall pressures in such flows may give data from which $F$ can be inferred accurately. This, too, seems worthy of future investigation.

## Acknowledgements

This work is associated with Australian Research Council grant DP140100094. I am grateful for the comments of four anonymous referees, which helped correct a misapprehension in an earlier draft of this paper.

## Appendix A. The solution algorithm

When equation (3.3) is multiplied by basis functions $\phi_k(z)$ and integrated, it requires the evaluation of the integrals

$$\begin{aligned} S^{(1)}_{nk} &= \int_{-1}^{1} z\phi_n(z)\phi_k(z)\,dz, \\ S^{(2)}_{nk} &= \int_{-1}^{1} z\psi'_n(z)\phi_k(z)\,dz, \\ S^{(3)}_{nk} &= \int_{-1}^{1} \psi_n(z)\phi_k(z)\,dz, \\ S^{(4)}_{nk} &= \int_{-1}^{1} \phi'_n(z)\phi_k(z)\,dz, \\ S^{(5)}_{nk} &= \int_{-1}^{1} \psi''_n(z)\phi_k(z)\,dz. \end{aligned} \tag{A.1}$$

Similarly, the second equation (3.4) multiplied by functions $\cos((k\pi/2)(z+1))$ and integrated requires the quantities

$$\begin{aligned} C^{(1)}_{nk} &= \int_{-1}^{1} z\psi_n(z)\cos\left(\frac{k\pi}{2}(z+1)\right)dz, \\ C^{(2)}_{nk} &= \int_{-1}^{1} \phi_n(z)\cos\left(\frac{k\pi}{2}(z+1)\right)dz, \\ C^{(3)}_{nk} &= \int_{-1}^{1} z\phi'_n(z)\cos\left(\frac{k\pi}{2}(z+1)\right)dz, \\ C^{(4)}_{nk} &= \int_{-1}^{1} \psi'_n(z)\cos\left(\frac{k\pi}{2}(z+1)\right)dz, \\ C^{(5)}_{nk} &= \int_{-1}^{1} \phi''_n(z)\cos\left(\frac{k\pi}{2}(z+1)\right)dz, \\ C^{(6)}_{nk} &= \int_{-1}^{1} \psi'''_n(z)\cos\left(\frac{k\pi}{2}(z+1)\right)dz \end{aligned} \tag{A.2}$$

to be evaluated. The quadratures in these expressions (A.1), (A.2) are all performed exactly, so as to maintain accuracy. In the code, they are calculated as

$$\begin{aligned} S^{(1)}_{nk} &= \frac{2}{\pi^2}\left[\frac{1}{(n+k)^2} - \frac{1}{(n-k)^2}\right]\gamma_{nk}, \\ S^{(4)}_{nk} &= \frac{n}{2}\left[\frac{1}{(n+k)} - \frac{1}{(n-k)}\right]\gamma_{nk}, \\ C^{(2)}_{nk} &= \frac{1}{\pi}\left[\frac{1}{(n-k)} + \frac{1}{(n+k)}\right]\gamma_{nk}, \end{aligned} \tag{A.3}$$

https://doi.org/10.1017/S1446181115000176 Published online by Cambridge University Press

$$C^{(3)}_{nk} = -\frac{n}{\pi}\left[\frac{1}{(n-k)^2} + \frac{1}{(n+k)^2}\right]\gamma_{nk},$$
$$C^{(5)}_{nk} = -\frac{n^2\pi}{4}\left[\frac{1}{(n-k)} + \frac{1}{(n+k)}\right]\gamma_{nk}$$

for $n \neq k$, and zero otherwise. The remaining quantities are likewise evaluated to give

$$\begin{aligned}
S^{(2)}_{nk} &= \frac{1}{\pi}\left[n\left\{\frac{1}{(n-k)^2} - \frac{1}{(n+k)^2}\right\} + (n+2)\left\{\frac{1}{(n+2+k)^2} - \frac{1}{(n+2-k)^2}\right\}\right]\gamma_{nk}\\
S^{(3)}_{nk} &= \frac{1}{\pi}\left[\frac{1}{(n+k)} - \frac{1}{(n-k)} - \frac{1}{(n+2+k)} + \frac{1}{(n+2-k)}\right]\gamma_{nk}\\
S^{(5)}_{nk} &= \frac{\pi}{4}\left[n^2\left\{\frac{1}{(n-k)} - \frac{1}{(n+k)}\right\} - (n+2)^2\left\{\frac{1}{(n+2-k)} - \frac{1}{(n+2+k)}\right\}\right]\gamma_{nk}\\
C^{(1)}_{nk} &= -\frac{2}{\pi^2}\left[\frac{1}{(n-k)^2} + \frac{1}{(n+k)^2} - \frac{1}{(n+2-k)^2} - \frac{1}{(n+2+k)^2}\right]\gamma_{nk}\\
C^{(4)}_{nk} &= -\frac{1}{2}\left[n\left\{\frac{1}{(n-k)} + \frac{1}{(n+k)}\right\} - (n+2)\left\{\frac{1}{(n+2-k)} + \frac{1}{(n+2+k)}\right\}\right]\gamma_{nk}\\
C^{(6)}_{nk} &= \frac{\pi^2}{8}\left[n^3\left\{\frac{1}{(n-k)} + \frac{1}{(n+k)}\right\} - (n+2)^3\left\{\frac{1}{(n+2-k)} + \frac{1}{(n+2+k)}\right\}\right]\gamma_{nk}
\end{aligned} \tag{A.4}$$

for $n \neq k$ and $n \neq k-2$ and zero otherwise. In all these evaluated quadratures (A.3) and (A.4), it is convenient to define

$$\gamma_{nk} = 1 - \cos((n+k)\pi).$$

It is now possible to create the elements of the two matrices $\mathbf{P}$ and $\mathbf{Q}$ in the algorithm (3.8). For convenience, symbols

$$\xi^2 = K^2 + \Gamma^2 \quad \text{and} \quad \Delta_k = \xi^2 + \left(\frac{k\pi}{2}\right)^2$$

are defined (and the first of these was encountered in Section 4.2). It now follows, after some algebra, that the block matrices on the left-hand side of (3.8) have components

$$\begin{aligned}
P^{(1A)}_{kn} &= \xi^2\left[-i\left(S^{(1)}_{nk} - \frac{1}{F}S^{(4)}_{nk}\right) + \delta_{kn}\frac{\Delta_k}{R_eK}\right]\\
P^{(1B)}_{kn} &= \Gamma\left[S^{(3)}_{nk} - S^{(2)}_{nk} + \frac{1}{2F}\left(S^{(5)}_{nk} + \xi^2 S^{(3)}_{nk}\right) + \frac{i}{R_eK}\left(\frac{k\pi}{2}\right)\Delta_k\left(\delta_{kn} - \delta_{k-2,n}\right)\right]\\
P^{(2A)}_{kn} &= i\left[-K\left(C^{(2)}_{nk} + C^{(3)}_{nk}\right) - \frac{\Gamma^2}{2FK}\xi^2 C^{(2)}_{nk} + \frac{1}{2F}\left(\frac{\Gamma^2}{K} + 2K\right)C^{(5)}_{nk}\right] + \delta_{kn}\frac{1}{R_e}\left(\frac{k\pi}{2}\right)\Delta_k\\
P^{(2B)}_{kn} &= \Gamma\left[-KC^{(1)}_{nk} + \frac{1}{2FK}\{(K^2-\Gamma^2)C^{(4)}_{nk} + C^{(6)}_{nk}\} - \frac{i}{R_e}\Delta_k(\delta_{kn} - \delta_{k-2,n})\right],
\end{aligned} \tag{A.5}$$

in which the rows are represented by the index $k$ and columns by index $n$. In these expressions, the term $\delta_{kn}$ is the usual Kronecker delta, having value 1 when $k = n$ and

https://doi.org/10.1017/S1446181115000176 Published online by Cambridge University Press

zero otherwise. The block matrices on the right-hand side of equation (3.8) are simpler, and can be written as

$$\begin{aligned} Q_{kn}^{(1A)} &= \frac{i}{K}\xi^2\delta_{kn}, \\ Q_{kn}^{(1B)} &= -\frac{\Gamma}{K}\left(\frac{k\pi}{2}\right)(\delta_{kn} - \delta_{k-2,n}), \\ Q_{kn}^{(2A)} &= i\left(\frac{k\pi}{2}\right)\delta_{kn}, \\ Q_{kn}^{(2B)} &= \Gamma(\delta_{kn} - \delta_{k-2,n}). \end{aligned} \tag{A.6}$$

Although seemingly complicated, these expressions (A.3)–(A.6) are straightforward to code.

## References


[1] R. Aris, *Vectors, tensors, and the basic equations of fluid mechanics* (Dover Publications, New York, 1962).

[2] B. J. Bayly, S. A. Orszag and T. Herbert, "Instability mechanisms in shear-flow transition", *Annu. Rev. Fluid Mech.* **20** (1988) 359–391; doi:10.1146/annurev.fl.20.010188.002043.

[3] C. Cambon and J. F. Scott, "Linear and nonlinear models of anisotropic turbulence", *Annu. Rev. Fluid Mech.* **31** (1999) 1–53; doi:10.1146/annurev.fluid.31.1.1.

[4] S. Cherubini, P. De Palma, J.-Ch. Robinet and A. Bottaro, "A purely nonlinear route to transition approaching the edge of chaos in a boundary layer", *Fluid Dyn. Res.* **44** (2012) 1–11; doi:10.1088/0169-5983/44/3/031404.

[5] P. A. Davidson, *Turbulence. An introduction for scientists and engineers* (Oxford University Press, Oxford, 2004).

[6] P. G. Drazin and W. H. Reid, *Hydrodynamic stability*, 2nd edn (Cambridge University Press, Cambridge, 2004).

[7] B. Eckhardt, "Turbulence transition in shear flows: chaos in high-dimensional spaces", *Procedia IUTAM* **5** (2012) 165–168; doi:10.1016/j.piutam.2012.06.021.

[8] D. Faranda, V. Lucarini, P. Manneville and J. Wouters, "On using extreme values to detect global stability thresholds in multi-stable systems: the case of transitional plane Couette flow", *Chaos Solitons & Fractals* **64** (2014) 26–35; doi:10.1016/j.chaos.2014.01.008.

[9] L. K. Forbes, "On turbulence modelling and the transition from laminar to turbulent flow", *ANZIAM J.* **56** (2014) 28–47; doi:10.1017/S1446181114000224.

[10] J. S. Frederiksen, "Singular vectors, finite-time normal modes, and error growth during blocking", *J. Atmos. Sci.* **57** (2000) 312–333; doi:10.1175/1520-0469(2000)057<0312:SVFTNM>2.0.CO;2.

[11] W. P. Graebel, "Stability of a Stokesian fluid in Couette flow", *Phys. Fluids* **4** (1961) 362–368; doi:10.1063/1.1706334.

[12] A. Groisman and V. Steinberg, "Elastic turbulence in a polymer solution flow", *Nature* **405** (2000) 53–55; doi:10.1038/35011019.

[13] B. Hof, C. W. H. van Doorne, J. Westerweel, F. T. M. Nieuwstadt, H. Faisst, B. Eckhardt, H. Wedin, R. R. Kerswell and F. Waleffe, "Experimental observation of nonlinear traveling waves in turbulent pipe flow", *Science* **305** (2004) 1594–1598; doi:10.1126/science.1100393.

[14] J. Jiménez, "Turbulence", in: *Perspectives in fluid dynamics. A collective introduction to current research* (eds G. K. Batchelor, H. K. Moffatt and M. G. Worster), (Cambridge University Press, Cambridge, 2000) 231–288.

[15] V. Kitsios, L. Cordier, J.-P. Bonnet, A. Ooi and J. Soria, "Development of a nonlinear eddy-viscosity closure for the triple-decomposition stability analysis of a turbulent channel", *J. Fluid Mech.* **664** (2010) 74–107; doi:10.1017/S0022112010003617.

[16] R. G. Larson, "Fluid dynamics – turbulence without inertia", *Nature* **405** (2000) 27–28; doi:10.1038/35011172.
[17] K.-C. Lee and B. A. Finlayson, "Stability of plane Poiseuille and Couette flow of a Maxwell fluid", *J. Non-Newtonian Fluid Mech.* **21** (1986) 65–78; doi:10.1016/0377-0257(86)80063-5.
[18] G. E. Mase, "Continuum mechanics", in: *Schaum's outline series* (McGraw-Hill, New York, 1970).
[19] W. D. McComb, "Theory of turbulence", *Rep. Prog. Phys.* **58** (1995) 1117–1206; doi:10.1088/0034-4885/58/10/001.
[20] L. Pan, A. Morozov, C. Wagner and P. E. Arratia, "Nonlinear elastic instability in channel flows at low Reynolds numbers", *Phys. Rev. Lett.* **110** (2013) 174502; 5 pages; doi:10.1103/PhysRevLett.110.174502.
[21] R. J. Poole, "The Deborah and Weissenberg numbers. The British Society of Rheology", *Rheology Bulletin* **53** (2012) 32–39; http://pcwww.liv.ac.uk/~robpoole/PAPERS/POOLE_45.pdf.
[22] S. M. E. Rabin, C. P. Caulfield and R. R. Kerswell, "Triggering turbulence efficiently in plane Couette flow", *J. Fluid Mech.* **712** (2012) 244–272; doi:10.1017/jfm.2012.417.
[23] S. C. Reddy, P. J. Schmid and D. S. Henningson, "Pseudospectra of the Orr-Sommerfeld operator", *SIAM J. Appl. Math.* **53** (1993) 15–47; doi:10.1137/0153002.
[24] M. Reiner, "A mathematical theory of dilatancy", *Amer. J. Math.* **67** (1945) 350–362; http://www.jstor.org/stable/2371950.
[25] O. Reynolds, "An experimental investigation of the circumstances which determine whether the motion of water shall be direct or Sinuous, and of the law of resistance in parallel channels", *Proc. R. Soc. Lond.* **35** (1883) 84–99; doi:10.1098/rspl.1883.0018.
[26] O. Reynolds, "On the dynamical theory of incompressible viscous fluids and the determination of the criterion", *Philos. Trans. R. Soc. Lond. A* **186** (1895) 123–164; http://www.jstor.org/stable/90643.
[27] R. S. Rivlin, "The hydrodynamics of non-Newtonian fluids. I", *Proc. R. Soc. Lond. A* **193** (1948) 260–281; http://www.jstor.org/stable/97992.
[28] N. Rott, "Note on the history of the Reynolds number", *Annu. Rev. Fluid Mech.* **22** (1990) 1–11; doi:10.1146/annurev.fl.22.010190.000245.
[29] D. Samanta, Y. Dubief, M. Holzner, C. Schäfer, A. N. Morozov, C. Wagner and B. Hof, "Elasto-inertial turbulence", *Proc. Natl. Acad. Sci. USA* **110** (2013) 10557–10562; doi:10.1073/pnas.1219666110.
[30] E. S. G. Shaqfeh, "Purely elastic instabilities in viscometric flows", *Annu. Rev. Fluid Mech.* **28** (1996) 129–185; doi:10.1146/annurev.fl.28.010196.001021.
[31] C. G. Speziale, "On nonlinear $K$–$\ell$ and $K$–$\epsilon$ models of turbulence", *J. Fluid Mech.* **178** (1987) 459–475; doi:10.1017/S0022112087001319.
[32] H. B. Squire, "On the stability for three-dimensional disturbances of viscous fluid flow between parallel walls", *Proc. R. Soc. Lond. A* **142** (1933) 621–628; doi:10.1098/rspa.1933.0193.
[33] K. R. Sreenivasan, "Fluid turbulence", *Rev. Modern Phys.* **71** (1999) S383–S395; doi:10.1103/RevModPhys.71.S383.
[34] J. M. T. Thompson and H. B. Stewart, *Nonlinear dynamics and chaos* (Wiley Publications, New York, 1986).
[35] L. N. Trefethen, A. E. Trefethen, S. C. Reddy and T. A. Driscoll, "Hydrodynamic stability without eigenvalues", *Science* **261** (1993) 578–584; doi:10.1126/science.261.5121.578.
[36] J. V. Valério, M. S. Carvalho and C. Tomei, "Efficient computation of the spectrum of viscoelastic flows", *J. Comput. Phys.* **228** (2009) 1172–1187; doi:10.1016/j.jcp.2008.10.018.
[37] F. Waleffe, "Exact coherent structures in channel flow", *J. Fluid Mech.* **435** (2001) 93–102; doi:10.1017/S0022112001004189.
[38] H. J. Wilson, M. Renardy and Y. Renardy, "Structure of the spectrum in zero Reynolds number flow of the UCM and Oldroyd-B liquids", *J. Non-Newtonian Fluid Mech.* **80** (1999) 251–268; doi:10.1016/S0377-0257(98)00087-1.